

Rothamsted Repository Download

A - Papers appearing in refereed journals

Cheng, Q., Wang, S., Peng, T., Cao, L., Zhang, X., Buckerfield, S. J., Zhang, Y. and Collins, A. L. 2020. Sediment sources, soil loss rates and sediment yields in a Karst plateau catchment in Southwest China. *Agriculture, Ecosystems & Environment*. 304, p. 107114.
<https://doi.org/10.1016/j.agee.2020.107114>

The publisher's version can be accessed at:

- <https://doi.org/10.1016/j.agee.2020.107114>

The output can be accessed at:

<https://repository.rothamsted.ac.uk/item/981xz/sediment-sources-soil-loss-rates-and-sediment-yields-in-a-karst-plateau-catchment-in-southwest-china>.

© 11 August 2020, Please contact library@rothamsted.ac.uk for copyright queries.

1 **Sediment sources, soil loss rates and sediment yields in a Karst plateau**
2 **catchment in Southwest China**

3
4 Qianyun Cheng^{a, b}, Shijie Wang^a, Tao Peng^{a*}, Le Cao^{a, b}, Xinbao Zhang^c, Sarah J.
5 Buckerfield^{d, e}, Yusheng Zhang^f, Adrian L. Collins^f

6
7 *^a State Key Laboratory of Environment Geochemistry, Institute of Geochemistry,*
8 *Chinese Academy of Sciences, Guiyang 550081, China;*

9 *^b University of Chinese Academy of Sciences, Beijing 100049, China;*

10 *^c Institute of Mountain Hazards and Environment, Chinese Academy of Sciences,*
11 *Chengdu 610041, China.*

12 *^d Biological and Environmental Sciences, Faculty of Natural Sciences, University of*
13 *Stirling, Stirling FJ9 4LA, UK.*

14 *^e Institute of Surface-Earth System Science, Tianjin University, Tianjin 300072,*
15 *China.*

16 *^f Sustainable Agriculture Sciences Department, Rothamsted Research, North Wyke,*
17 *Okehampton EX20 2SB, UK*

18
19 Corresponding author: Tao Peng

20 E-mail: pengtao@mail.gyig.ac.cn

21

22

23 **Abstract**

24 Intensive agricultural activities have accelerated soil erosion and rocky
25 desertification in karst regions of southwest China. Knowledge of sediment sources and
26 soil erosion rates can be used to target soil conservation measures and to improve
27 calibration and validation of process-based soil erosion and sediment delivery models
28 for scenario analyses. Due to the complexity of karst environments, however,
29 catchment scale information on these components of sediment budgets has rarely been
30 assembled, meaning there continues to be an evidence gap. Within this context, this
31 study selected Chenqi catchment, given its appropriate research infrastructure, to
32 investigate sediment sources and soil loss rates in a typical karst agroforestry landscape.
33 We estimated the relative contributions from three sources: surface soil, subsurface soil
34 and clastic rock, using a composite fingerprinting procedure combining ^{137}Cs and
35 magnetic susceptibility and a frequentist un-mixing model with Monte Carlo
36 uncertainty analysis. Suspended sediment samples were taken at an hourly interval
37 during seven rainfall events in 2017-2018 to characterize and quantify the sediment
38 exported in both surface and underground drainage. The overall average median
39 contributions (with 5th-95th percentile uncertainty ranges) from the sources to the
40 suspended sediment samples from the surface drainage outlet were in the order: 62%
41 (0-99%) subsurface soils, 25% (0-91%) surface soils and 13% (0-45%) clastic rock. For
42 the sediment samples collected from the underground drainage catchment outlet, the
43 corresponding estimates were in the order: 68% (0-97%) subsurface soils, 25% (0-53%)
44 clastic rock and 7% (0-44%) surface soils. Plot scale soil loss rates were highest on

45 cropland (0.70 Mg km⁻²) and pasture land (0.48 Mg km⁻²). The average (2017 and 2018)
46 annual suspended sediment load exported through the surface outlet was 4.64 Mg km⁻²
47 compared with 1.20 Mg km⁻² through the underground outlet. The broader implications
48 of this study are that subsurface and clastic rock sources represent a significant
49 component of the catchment sediment budget, meaning erosion control measures
50 targeting hillslope surface soils alone may have limited impact on suspended sediment
51 export at landscape scale.

52 **Keywords:** sediment source; fingerprinting; ¹³⁷Cs; magnetic susceptibility; karst;
53 headwater catchment; critical zone

54

55 1. Introduction

56 Due to population pressure, the increasing intensity of human exploitation of the land
57 has changed the landscape structure of karst areas and accelerated the speed of soil
58 degradation, depletion of fertility, rocky desertification and reduction of biodiversity.
59 This has resulted in the ongoing conflict between ecological protection and socio-
60 economic development in karst areas (Hartmann *et al.*, 2014; Cao *et al.*, 2015; Li *et al.*,
61 2017). Currently, rocky desertification caused by soil erosion in karst areas is
62 highlighted as one serious ecological problem in southwest China, which not only
63 restricts the sustainable development of the economy, but also directly threatens the
64 ecological security of the Yangtze River and Pearl River basins (Peng and Wang, 2012;
65 Jiang *et al.*, 2014a; Martin *et al.*, 2016; Dai *et al.*, 2017). In karst environments, soils
66 are often very thin and rocky, and channels in the underlying bedrock, apertures, and

67 solution-enlarged fissures facilitate the transport of mobilized sediment from the land
68 surface to underground systems. As a result, the lack of soil for cultivation severely
69 threatens sustainable agriculture (Williams, 1983; White, 2007; Wilcox *et al.*, 2007).

70 According to the 2018 national water and soil conservation bulletin, the total area of
71 soil and water conservation measures in China was 9,916,196 km², whilst that in the
72 eight karst provinces in southwest China was 3,302,593 km². Hillslope farmland,
73 considered as the main source area of soil erosion, is currently the target for soil erosion
74 protection measures since this source accounts for ~1/3 of the total soil erosion in China
75 (Ministry of water resources, 2010). It is therefore considered to be of great importance
76 to strengthen comprehensive control of soil loss on hillslope farmland, including in the
77 karst regions of southwest China. However, sediment dynamics in karst regions are still
78 unclear due to the extreme heterogeneity in the lithological and hydrological properties
79 of well-developed karst. Understanding the provenance of suspended sediment
80 exported from such catchments with various land use types can help understand how
81 different agricultural activities and intrinsic landscape features and processes influence
82 erosion rates and sediment source dynamics. Such information is needed to provide a
83 more robust evidence base for selecting measures to control soil erosion, conserve soil
84 and water resources, manage watersheds, and promote effective ecological restoration
85 in karst areas.

86 Generally, soil migration downwards through pores and fissures into the joints and
87 conduits which characterize karst aquifers and which provide rapid flow pathways,
88 results in subsurface soil loss being an important soil erosion mechanism in karst

89 landscapes (Yuan, 1997; Li *et al.*, 2002; Zhang *et al.*, 2007; Dai *et al.*, 2015). However,
90 the relative importance of surface soil erosion versus underground soil loss and indeed,
91 in the context of additional sources, is still widely debated for the karst region in
92 southwest China. Research on the ratio between surface and underground soil loss has
93 still not resulted in consensus (Zhang *et al.*, 2011; Zhou *et al.*, 2012; Peng *et al.*, 2013;
94 Wei, 2013). Some researchers argue that underground soil loss is the main process of
95 soil erosion (Jiang *et al.*, 2014b; Li and Wu, 2015), while others suggest that surface
96 soil loss is dominant because there is a greater volume of soil that can be eroded from
97 farmed hillslopes rather than rock fissures (Wang *et al.*, 2014; Wei *et al.*, 2016). Besides,
98 [the lithology and landscape characteristics](#) in karst catchments have recently been
99 shown to have a strong influence on sediment yields, due to their effect on erosion
100 mechanisms (Li *et al.*, 2019). Karst catchments display a wide variation in lithology,
101 from pure carbonate to carbonate highly intercalated with clastic rocks of varying
102 solubility and erosivity. The higher concentration of insoluble components in non-
103 carbonate rocks makes intercalated layers a possible intrinsic source of suspended
104 sediments in karst areas, where the majority of carbonate rocks are highly soluble (Feng
105 *et al.*, 2014). However, this aspect of karst lithology, and the corresponding
106 consequences for erosion and sediment source dynamics, has not been addressed; the
107 easily erodible soils, rather than the insoluble clastic material have been the main focus
108 of previous studies concerning the contributions of different sediment sources. Due to
109 this heterogeneity and complexity in the erosivity of carbonates intercalated with clastic
110 material, and [the important role that clastic sediments plays in sediment transport and](#)

111 storage in karst landscapes (Bonacci, 1987), clastic rock pieces should be considered as
112 one of the sediment sources and thus traditional measurement techniques may not be
113 suitable for elucidating suspended sediment provenance, since these methods are not
114 pragmatic for dealing with the often pronounced spatio-temporal variability of erosion
115 and sediment delivery pathways.

116 Sediment fingerprinting has therefore been increasingly used as a tool for
117 discriminating and apportioning sediment sources and erosion mechanisms in a range
118 of geological and land use settings (Collins *et al.*, 2010; Gellis and Walling, 2011;
119 Miller *et al.*, 2015; Owens *et al.*, 2016; Collins *et al.*, 2017). On this basis, fingerprinting
120 methods may be a suitable approach to estimating sediment sources in karst catchments
121 with dual-structure (i.e., surface and underground) drainage systems. Where such
122 information can be integrated with measured sediment export, it is possible to quantify
123 the magnitude of the net sediment loss from individual sources successfully
124 discriminated by the source fingerprinting approach.

125 Fallout radionuclides and mineral magnetic properties are two types of tracer
126 properties that have previously been used successfully to apportion sediment sources
127 using the fingerprinting approach. ^{137}Cs ($t_{1/2}=30.2$ years) has been included in many
128 studies as a fingerprint property to distinguish sediment sources associated with
129 different depths (Russell *et al.*, 2001; Matisoff *et al.*, 2002; Nagle and Ritchie, 2004;
130 He *et al.*, 2009). The concentration of ^{137}Cs is independent of soil type and underlying
131 geology, making it an appropriate source fingerprinting property in heterogeneous
132 catchments such as those with karstic bedrock. Magnetic properties (namely magnetic

133 susceptibility) can be particularly useful in constraining the origin of sediment, since
134 the magnetic susceptibility of soils is linked to the degree of weathering and soil erosion
135 (Gennadiev *et al.*, 2002; Olson *et al.*, 2002; Sadiki *et al.*, 2009; Ayoubi *et al.*, 2012;
136 Rahimi *et al.*, 2013; Jordanova *et al.*, 2014). It was therefore deemed logical to test
137 these properties in applying the source fingerprinting approach in a typical karst
138 catchment. More specifically, the objectives of this study were: (i) to identify the
139 principal sources of the suspended sediment exported from a typical agro-forestry karst
140 catchment in southwest China using catchment-specific composite source
141 fingerprinting including an un-mixing model with uncertainty analysis, and; (ii) to
142 integrate the source fingerprinting estimates with measurements of sediment export to
143 quantify the magnitude of net sediment loss from individual sources, and (iii) to
144 describe how agricultural activities influence the soil erosion processes in karst areas.

145

146 **2. Materials and methods**

147 **2.1. Study area**

148 The study area, Chenqi catchment (1.3 km²; 26°15'36"N, 105°43'30"E), is located in
149 Puding County, Guizhou Province, southwest China. It is part of the Wujiang River
150 catchment of the Yangtze River basin (Fig. 1). Chenqi has an altitude range of 1316 m
151 to 1500 m a.s.l. The region has a subtropical monsoonal climate with an annual mean
152 temperature of 14 °C and total precipitation of 1336 mm. The temperature ranges from
153 an average minimum of -1 °C to an average maximum of 28 °C, and over 80% of the
154 rain in any year falls between May and October. The study area is a typical karst

155 agroforestry catchment of the central Guizhou plateau, containing a range of karstic
156 landforms, including karst gullies, dry valleys and small karst caves. The valley
157 depression with a thick soil profile is used for paddy cultivation, whereas the gentle
158 hillslopes are used for the cultivation of other crops. Steeply sloping hillslopes are
159 partially grazed but were also partially re-forested in conjunction with land conversion
160 under the 'Grain for Green' project in the 1990s (Jintao, 2004).

161 The lithology is mainly thick bioclastic limestone strata of the Middle Triassic
162 Guanling Formation with thin interbeds of muddy limestone (Fig. 2). Clastic rock
163 pieces are contained within silicate interbeds and the carbonate strata. The primary
164 drainage networks for the surface and underground catchments are spatially very
165 similar. A surface river that has been fully contained within concrete channeling runs
166 from the eastern slopes through the valley depression to the outlet in the west, receiving
167 discharge from numerous gullies draining the hillslopes. The primary groundwater
168 channel follows a similar geometry. The underground outlet is a rising spring at the
169 mudstone aquitard layer, and the surface outlet is an ephemeral stream. A hydrological
170 station at the catchment outlet measures discharge at a 5-minute interval from both the
171 underground and surface water outlets. There are six bounded runoff fields distributed
172 on the slopes of the study catchment (Fig.1), representing different land uses including
173 the recovered land after burning (BAR), the non-recovered land after burning (BAU),
174 combined vegetation land (CVL), continued cropland (CL), young forestland (YFL),
175 and pastureland (PL) (Peng and Wang, 2012).

176

177 **2.2. Soil and sediment sampling**

178 Three potential sediment sources were sampled during the dry season from
179 December 2016 to April 2017, yielding 16 surface soil samples from hillslopes, 13
180 subsurface soil samples and six clastic rock samples. The distribution of the source
181 samples is shown in Fig. 1. The surface soil was collected from a depth of 0-5 cm in
182 areas with four types of land use comprising forest, pastureland, slope cropland, and
183 paddy fields. Each sample was a composite of five subsamples collected from a two-
184 meter radius of the sampling point using a wooden shovel. The subsurface soil samples
185 were collected from eroding gully banks and from rock fissures. Three subsamples with
186 different depths (excluding the topsoil part) from the gully banks or the fissures were
187 composited in each subsurface soil sample. The clastic rock pieces were collected from
188 slopes where the interbedded mudstone layers outcrop. Undissolved clastic rock was
189 included as a potential sediment source following published reviews for karst systems
190 (Herman *et al.*, 2012; Herman, 2012; Hartmann *et al.*, 2014).

191 Suspended sediment samples were collected from the surface and underground
192 outlets during seven heavy rainfall events in the wet seasons of 2017 and 2018. In 2017,
193 we found that hourly samples did not yield sufficient sediment mass for ^{137}Cs analysis.
194 Thus, to retrieve sufficient sample mass, bulk (200 L) water samples were collected
195 with a large bucket every 30~60 minutes during the storms sampled in 2018. For those
196 sediment samples with less mass collected in 2017, samples from two runoff events
197 with similar rainfall characteristics were bulked to permit laboratory analysis of this
198 particular sediment tracer.

199

200 **2.3. Laboratory analyses**

201 A Beckman Coulter LS3320 laser diffraction particle analyzer was used to measure
202 the particle size of suspended sediment samples. Before the test, 10% H₂O₂ was added,
203 according to the sample volume and sediment concentration, to remove the organic
204 matter in the sample. Here, the solution was heated to boiling point, then the carbonate
205 was removed by adding 10% HCl. Finally, 0.25 mol/L Na₂P₂O₇ was added for full
206 dispersion of the sediment sample. The results of the laser diffraction particle size
207 analysis were used to select the most appropriate mesh size (63 μm) for sieving the
208 samples collected in the study catchment to assist direct comparisons of tracer contents.

209 Source material samples were dry-sieved to <63 μm while suspended sediments were
210 wet-sieved to <63 μm and oven dried at 45°. Analyses for ¹³⁷Cs and magnetic
211 susceptibility were undertaken only on the sieved (<63 μm) particle size fraction of the
212 source material and suspended sediment samples. Since the source and suspended
213 sediment samples were sieved to the same specific particle size fraction, an additional
214 correction factor (e.g., (He and Walling, 1996)) for selectivity during erosion and
215 sediment delivery was not utilized.

216 ¹³⁷Cs activities in the source material and sediment samples were measured using a
217 gamma-ray spectrometer and detected at 662 keV. Count times for each sample
218 exceeded 33,000s, providing results with an analytical precision of approximately ±5%
219 at the 90% level of confidence. The magnetic susceptibility of the source material and
220 suspended sediment samples was measured by using a Bartington MS2B dual-

221 frequency magnetization meter (low frequency 470Hz, high frequency 4,700 Hz). Here,
222 we focused on measuring the low frequency mass-specific magnetic susceptibility,
223 since this provided a composite measurement of the total magnetic and non-magnetic
224 constituents with each sample, providing results with an analytical precision up to 0.1
225 $\times 10^{-5}$ SI and a relative error of 1%.

226

227 *2.4. Sediment source discrimination and ascription*

228 With respect to data processing, the two key stages concern source discrimination,
229 followed by source apportionment. Prior knowledge of tracer behaviour is helpful when
230 considering the most appropriate tracer for a given environmental setting (Collins *et*
231 *al.*, 2017). Tracers with small differences between source groups should be rejected as
232 they generate larger uncertainties in the estimated source proportions than tracers with
233 greater between-group contrasts (Collins and Walling, 2002). Additionally, tracers used
234 in composite fingerprints should show conservative behaviour during mobilization and
235 delivery through the study catchment. This can be tested using biplots of tracer pairings
236 which is considered to provide a more sensitive test for tracer conservatism (Pulley and
237 Collins, 2018; Nosrati and Collins, 2019) than the conventional range or bracket test
238 (Foster and Lees, 1999).

239 The frequentist numerical mass balance model of Collins *et al.* (2010a) was used to
240 calculate the relative contributions from each source, by using the function in Eq.1:

$$241 \text{RSS} = \sum_{i=1}^n \left\{ \left[\frac{C_{ssi} - \left(\sum_{s=1}^m P_s C_{sj} \right)}{C_{ssi}} \right]^2 W_i \right\} \quad (1)$$

242 where: C_{ssi} = deviate median concentration of fingerprint property (i) in target surface

243 or subsurface sediment samples; P_s = the optimized percentage contribution from
244 source category (s); C_{si} = deviate median concentration of fingerprint property (i) in
245 source category (s); W_i = the tracer discriminatory power weighting.

246 Uncertainty ranges for the predicted source proportions were determined using a
247 Monte Carlo sampling routine (Collins *et al.*, 2012; Theuring *et al.*, 2015). Here, the
248 model input probability density functions representing the tracer values in the source
249 categories were constructed using the mean and Qn (Rousseeuw and Croux, 1993) for
250 each tracer. Similarly, probability density functions were constructed in the same
251 manner to represent the tracer values in either the surface or subsurface target sediment
252 samples. The mixing model was run until 5000 iterations satisfied a threshold for
253 absolute mixing model error of $\leq 20\%$. One batch run was undertaken for the surface
254 sediment samples, and another for the subsurface sediment samples.

255 To evaluate the predicted source proportions for either the surface or subsurface
256 sediment samples, virtual mixture tests were performed since this is now established as
257 a standard, but important, methodological step in source fingerprinting studies (Palazón
258 *et al.*, 2015; Collins *et al.*, 2017; Pulley and Collins, 2018; Nosrati and Collins, 2019).
259 More specifically, 20 virtual mixtures were generated with different proportions of the
260 three sources under scrutiny. The proportions were 0.05, 0.15, 0.3, 0.5, 0.7, 0.85 and
261 0.95 and a stratified sampling approach was employed whereby one source was
262 assigned a specified value from this list and the remaining two sources were assigned
263 equal shares of the remaining proportion. For example, one virtual mixture could have
264 a specified proportion of 0.3 for one source, with the other two sources assigned the

265 same proportion (0.35 each) in order to meet the underpinning mixing model
266 assumption that all source contributions should sum to unity. The Q_n values of the
267 tracer properties were assumed to be same as the Q_n values estimated for either all the
268 surface or subsurface sediment samples. Scatter plots of the actual known source
269 proportions and the predicted proportions for the three sources were plotted for
270 comparison and assessment of the mixing model accuracy.

271

272 2.5. *Measuring hillslope runoff*

273 Surface runoff and soil loss on the study catchment hillslopes with different land use
274 were monitored using the large bounded runoff field method. Since the hillslope area
275 accounts for 75% of the total area of the study catchment, monitoring the runoff and
276 soil erosion of these fields was assumed to provide a reasonable approximation of
277 surface soil erosion in the study catchment. More specifically, runoff and mobilized
278 sediment were collected in sedimentation tanks during storm events (see locations in
279 Fig. 1). Each tank was coupled to a square shaped collection pond (Peng and Wang,
280 2012). The runoff in the square pools was designed to represent one-eighth of the total
281 runoff generated on the fields (based on surface area). The volume of the runoff in the
282 tanks and square pools was measured after each rainfall event, and a 500 mL sample
283 was retrieved from each of the square pools after stirring and mixing of the collected
284 water-sediment mix, to provide an estimate of the sediment concentration in the
285 hillslope runoff. The soil erosion on hillslopes associated with each rainfall event could
286 thus be obtained. Additionally, the mobilized material reaching the tanks and pools was

287 retrieved, filtered and weighed in case of the need for further geochemical analysis. The
288 total erosion loss was calculated by adding the results for every sampled rainfall event.
289

290 **2.6. Discharge and sediment load monitoring at the study catchment outlet**

291 The turbidity in the surface and underground catchment outlets was monitored, in
292 situ, at a 10-minute interval using a VisoTurb@700IQ online turbidity analyzer
293 manufactured by WTW (NTU range 0-300; NTU precision 0.1). The rating relationship
294 between turbidity and gravimetrically-filtered suspended sediment concentration was
295 derived and the overall suspended sediment yield calculated using the following
296 empirical equation (3):

$$297 \quad M = \frac{1}{1000} \sum_{i=1}^n (aX + b) \times Q \times T \quad (3)$$

298 where: M = suspended sediment load, kg; n = frequency; a = slope coefficient in the
299 rating equation; X = turbidity, NTU; b = intercept coefficient in the rating equation; Q
300 = flow rate, m³/s; T = time resolution, s.

301

302 **3. Results**

303 **3.1. Sample characteristics and rainfall event data**

304 The suspended sediment samples from the surface and subsurface water outlets
305 showed that the <63 µm particle size fraction constituted over 85% of the suspended
306 sediment samples collected in both the surface and subsurface flows (Table 2). Using
307 the <63 µm particle size fraction was thus considered reasonable for the objective of
308 this study.

309 The concentrations of ^{137}Cs and the magnetic susceptibility of the three source types
310 are shown in Table 1. In the case of the surface soil samples, there was no significant
311 difference in either the ^{137}Cs or magnetic susceptibility among the different land uses
312 (Table 3). ^{137}Cs values in the sampled surface soils were highest, ranging from 2.28 to
313 4.77 Bq/kg, with a corresponding average of 3.39 Bq/kg, because ^{137}Cs is enriched in
314 surface soils due to fallout associated with atmospheric weapons testing during the
315 1950s-1970s. In contrast, the subsurface soil samples had low values of ^{137}Cs , ranging
316 from 0.00 to 0.65 Bq/kg with a corresponding average value of 0.50 Bq/kg, because
317 subsurface soils are either beneath surface soils in gully walls or deeply buried in karst
318 fissures and thereby receive less atmospheric fallout. There was no detectable ^{137}Cs in
319 the clastic rock pieces (Table 1) because this material has had no exposure to the
320 atmospheric fallout.

321 Unlike ^{137}Cs , the magnetic susceptibility of soil is a comprehensive reflection of soil
322 forming factors and processes. The surface soil, subsurface soil and clastic rock pieces
323 have experienced different environmental transformation. Accordingly, the magnetic
324 susceptibility data can provide useful information for source discrimination and
325 apportionment. The surface soil had high magnetic susceptibility (Table 1), ranging
326 between $205.11 \cdot 10^{-8} \text{ m}^3/\text{kg}$ and $370.13 \cdot 10^{-8} \text{ m}^3/\text{kg}$, with a corresponding average of
327 $310.07 \cdot 10^{-8} \text{ m}^3/\text{kg}$. The magnetic susceptibility of subsurface soil (Table 1) was slightly
328 lower, ranging from $145.28 \cdot 10^{-8} \text{ m}^3/\text{kg}$ to $198.50 \cdot 10^{-8} \text{ m}^3/\text{kg}$, with an average value of
329 $180.69 \cdot 10^{-8} \text{ m}^3/\text{kg}$. The magnetic susceptibility of clastic rock pieces was extremely low,
330 ranging between $5.50 \cdot 10^{-8} \text{ m}^3/\text{kg}$ and $7.90 \cdot 10^{-8} \text{ m}^3/\text{kg}$, with an average of $7.02 \cdot 10^{-8}$

331 m³/kg. The magnetic susceptibility of the samples collected in the study area was
332 consistent with the magnetic parameters of the soil profiles of carbonate rocks in
333 Guizhou province published by previous studies (Lu, 2003). Here, the higher magnetic
334 susceptibility of the surface soil is likely to be due to a high degree of weathering, with
335 the subsurface soil having a lower magnetic susceptibility than the surface soil, and the
336 basement carbonate rock having the lowest magnetic susceptibility. Overall, the
337 magnetic susceptibility data for the three sources indicates that this tracer is closely
338 related to weathering intensity and the soil forming environment.

339 Table 4 presents summary data for the rainfall events sampled during this study. The
340 highest rainfall event total precipitation was 50.2 mm. The maximum I₃₀ was 39.2 mm
341 h⁻¹. The total kinetic energy calculated for the individual rainfall events ranged between
342 3.71 and 9.69 J m⁻². The rainfall erosivity ranged between 29.76 and 193.80 J mm⁻¹ m²
343 hr⁻¹.

344

345 **3.2. Sediment source discrimination and apportionment**

346 The Kruskal-Wallis H-test indicated that both ¹³⁷Cs and magnetic susceptibility were
347 significantly different ($p < 0.05$) among surface soil, subsurface soil and clastic rock
348 samples (Table 5). The results in Table 6 confirm that our composite fingerprint
349 correctly classified 100% of the source samples. Biplots of tracer pairings (Figures 3
350 and 4) showed that magnetic susceptibilities with both high and low frequency were
351 conservative since all samples plot along the same line, whilst ¹³⁷Cs and mineral
352 magnetic properties plot within the same space, again indicating conservative

353 behaviour.

354 The estimated average median relative contributions (with corresponding 5th – 95th
355 percentile ranges) from the three source types to the catchment surface and underground
356 sampled suspended sediment loads are presented in Table 7. The overall average
357 median contributions from the catchment sources to the suspended sediment samples
358 collected in the surface drainage outlet were estimated at: 62% (0-99%) subsurface soils,
359 25% (0-91%) surface soils and 13% (0-45%) clastic rock. For the sediment samples
360 collected in the underground drainage catchment outlet, the corresponding estimates
361 were estimated to be: 68% (0-97%) subsurface soils, 25% (0-53%) clastic rock and 7%
362 (0-44%) surface soils. For both, the surface and underground drainage outlets, the
363 subsurface soils were therefore identified as the dominant suspended sediment source
364 during the 2017-2018 study period. Eroding surface soils were identified as being a
365 more important source of the suspended sediment samples collected from the surface
366 drainage pathway, rather than the underground catchment outlet. Source fingerprinting
367 suggested that clastic rock contributions were higher for the suspended sediment
368 samples collected from the underground drainage pathway.

369 Figure 5 summarizes the results of the virtual mixture tests comparing known and
370 predicted contributions from the individual sources. These results show that the un-
371 mixing model performed best for the surface soil (errors up to ~15%) and clastic rock
372 (errors up to ~5%) sources and least well for the subsurface source category (errors up
373 to ~19%).

374

375 **3.3. Annual surface soil loss from different land uses and the catchment suspended**
376 **sediment yields**

377 Table 8 shows the estimated soil loss for the six types of land use on the karst
378 hillslopes measured in 2017 and 2018. The CL and PL had the greatest soil loss rates,
379 followed by the BAR, with the BAU and CVL having no measured soil loss. We
380 calculated the annual sediment loads from the outlets for the water years 2017 and 2018.
381 The annual sediment loads from the surface outlet were calculated to be 4.08 Mg/km²
382 and 5.19 Mg/km² in 2017 and 2018, respectively. The corresponding annual sediment
383 loads exported along the underground pathway were 1.00 Mg/km² and 1.40 Mg/km² in
384 2017 and 2018, respectively. Combined with the estimated source proportions (Table
385 7), in the case of the surface outlet, the total net sediment loss from eroding subsurface
386 soils during the two sampling years was 5.75 Mg/km² (2.53 Mg/km² in 2017 and 3.22
387 Mg/km² in 2018). The corresponding estimate for surface soils was 2.32 Mg/km² (1.02
388 Mg/km² in 2017 and 1.30 Mg/km² in 2018). In the case of the clastic rock sediment
389 source, the corresponding estimate was 1.2 Mg/km² (0.53 Mg/km² in 2017 and 0.67
390 Mg/km² in 2018). For the underground sediment export pathway, the corresponding
391 estimates were 1.63 Mg/km² (0.68 Mg/km² in 2017 and 0.95 Mg/km² in 2018) from
392 eroded subsurface soils, 0.17 Mg/km² (0.07 Mg/km² in 2017 and 0.10 Mg/km² in 2018)
393 from eroded surface soils, and 0.6 Mg/km² (0.25 Mg/km² in 2017 and 0.35 Mg/km² in
394 2018) from clastic rocks.

395

396 **4. Discussion**

397 **4.1 Soil erosion features and sediment sources in the karst agroforestry catchment**
398 **system**

399 Our study indicates that the combination of the underlying geological strata and
400 overlying land-use, is the first order control on soil erosion and sediment source. The
401 subsurface soil source contributed most of the sampled suspended sediments. More than
402 half of the material sampled in both the surface flow and from the underground outlet
403 were predicted to come from the subsurface sources. The subsurface soil source consists
404 of two primary components; soil in the underground system and material eroded from
405 gully or river banks. Field observations suggested that the mobilization of subsurface
406 soil from gully/channel wall erosion during floods is important, especially in the case
407 of the subsurface soil contribution to the suspended sediment samples collected in the
408 surface drainage outlet. In contrast, the main contribution of the subsurface source to
409 the underground outlet sediment samples is more likely to be the result of soil from
410 rock fissures delivered into the underground river system through the dissolving
411 fissures; an underground leakage process unique to karst landscapes. Gully erosion in
412 small catchments is often characterized by deep sidewalls and steep profiles, and can
413 be an important suspended sediment contributor (Poesen *et al.*, 2003; Mararakanye and
414 Sumner, 2017). For example, it has been estimated that gully erosion could contribute
415 60% to 90% of the total sediment yield in the hilly region of the Chinese Loess Plateau
416 (Wang *et al.*, 2003; Ni *et al.*, 2017). Surface runoff in karst constitutes a minor
417 proportion of total rainwater flux. Instead, most of the rainwater seeps down into the
418 underground fissured structures through the porous lithology. Flushing of underground

419 soils thus occurs when there is high-intensity runoff moving quickly downwards
420 through cracks and fissures during rainfall events, accounting for most of the sampled
421 suspended sediment in our karst catchment. Such pathways and source contributions
422 are highly likely to be more generally representative of the karst catchments in
423 southwestern China.

424 Surface soils consistently contributed less to the suspended sediment samples. The
425 surface soils from both hillslopes and paddy land contributed little to the sampled
426 suspended sediment collected in the surface outlet because there was limited surface
427 runoff on the hillslopes and where it was observed, it only transported detached soil
428 short distances during rain storms. Other studies (Chen *et al.*, 2008; Peng *et al.*, 2008;
429 Peng *et al.*, 2011; Chen *et al.*, 2012; Zhang *et al.*, 2014) have reported that surface
430 runoff processes are insignificant for soil erosion in karst landscapes, and that
431 underground erosion, remobilization, and underground runoff are, instead, the main
432 processes responsible for sediment transport in karst terrain. This is not an unexpected
433 result considering that subsurface pore space and fissures provide pathways for runoff,
434 resulting in high permeability at the land surface in karst landscapes (Fu *et al.*, 2015).
435 Due to the limited surface runoff, limited sediment transport can occur on slope surfaces,
436 which results in a lower contribution (relative to subsurface soils) to sampled suspended
437 sediments at this headwater catchment scale.

438 The clastic rock outcrops were the least significant suspended sediment source for
439 both the surface and underground hydrological outlets. Mudstone interbedded with the
440 carbonate strata in the middle section of the Guanling Formation forms impermeable

441 layers in our study catchment, preventing infiltration of fracture-hosted water. When
442 large volumes of precipitation infiltrate the epikarst during heavy rainfall events in the
443 wet season, the mudstone aquitard layers block infiltration and cause horizontal flow
444 and water emergence at epikarst springs (Bonacci, 1987). As a result, erosion occurs at
445 the mudstone-carbonate interface and muddy intercalated debris is transported to the
446 river system. By way of comparison, albeit on a different lithology, previous work in
447 the Huangfuchuan catchment on the northern Loess Plateau, has estimated the
448 contribution from easily eroded coarse sandstone (the Pisha sandstone) which
449 constitutes a small fraction of the local lithological strata. In this case, it contributed
450 more than half of the dam infill sediment deposits associated with 31 rainfall events
451 over the period 1958-1972 (Zhao *et al.*, 2015; Zhao *et al.*, 2017). Regardless of the
452 contrasts in the significance of clastic layers in karst or sandstone regions, our estimated
453 contributions from clastic rocks illustrates that suspended sediment sources in karst
454 catchments in southwestern China are influenced by the composition of the geological
455 strata.

456

457 ***4.2 Historical agricultural activity and rainfall as controls on present day sediment*** 458 ***sources and yields***

459 An interesting dimension to the interpretation of our findings concerns the issue of
460 legacy sediment mobilized from surface sources in the past. Between 1979 to 1981,
461 farmers cleared trees without restriction in some areas due to the adjustment of rural
462 land use rights, which resulted in severe soil erosion on sloping fields by surface runoff.

463 Deforestation to expand available farm land often triggered severe soil erosion in the
464 Guizhou karst plateau region due to high population pressure, and it has been estimated
465 that erosion rates on hillslopes could potentially have reached thousands of tones per
466 square kilometer every year after the period of deforestation and ensuing cultivation.
467 Here, for instance, a large amount of soil was eroded during the 1980s in southwest
468 China (Lin and Zhu, 1999; Zhang *et al.*, 2011). In addition, ^{137}Cs concentrations
469 measured in the soils of karst depressions (Zhang *et al.*, 2009) and in the sediment
470 deposits of reservoirs (Wan *et al.*, 1991; Wenbo *et al.*, 2008; Zhang *et al.*, 2009) indicate
471 that the soil eroded during the 1980s was very high in ^{137}Cs content. Research in karst
472 depressions near Chenqi catchment have also reported that, in 2007, the peak
473 concentration of ^{137}Cs could be as high as 7.25 Bq/kg in 2007 (Zhang *et al.*, 2010),
474 which would have diminished to 5.63 Bq/kg in 2018 based on known radionuclide
475 decay rates. Following the same theory, the average concentration of ^{137}Cs from the
476 field runoff sediments in the Chenqi study catchment in 2007 was 6.80 Bq/kg (Bai *et*
477 *al.*, 2009), which would diminish to 5.28 Bq/kg in 2018. When the rainfall erosivity
478 exceeded a certain point, $49.08 \text{ J}\cdot\text{mm}\cdot\text{m}^{-2}\cdot\text{h}^{-1}$, sediments stored in large volume
479 subterranean cavity spaces in karst can be remobilized out of the subsurface structure
480 and contribute as a source to suspended sediment sampled in the present day (i.e., our
481 study period). The old sediment eroded from the surface soils during and after
482 deforestation several decades ago is hence a contributor to the suspended sediment
483 exported from the catchment during contemporary heavy rainfall events. Figure 5
484 shows a schematic of how the historical soil erosion pathways (Figure 5a) changed

485 following deforestation and ensuing cultivation during the 1980s (Figure 5b). Soil
486 erosion during the years immediately following deforestation and ensuing cultivation
487 in our karst catchment mean that subsurface source contributions from rock fissures
488 now release legacy sediments during those rainstorms capable of flushing subterranean
489 stores. Measures to protect soil from erosion should be focused on the early years after
490 deforestation for hillslope farming. Where mitigation measures are not implemented
491 with sufficient timeliness, the movement of surface soil into underground rock fissures
492 generates a secondary source of legacy sediment which continues to be remobilized in
493 the present day, helping to account for the importance of subsurface sediment sources,
494 alongside the erosion of gully walls. An accurate threshold value to determine the risk
495 of remobilization of legacy sediment sequestered in underground structures such as
496 fissures could be identified through monitoring more rainfall events.

497

498 **5. Conclusion**

499 Rainfall characteristics, historical agricultural activity, bedrock lithology, and the
500 dual-structure of the karstic drainage system are all important controls on suspended
501 sediment dynamics in karst watersheds. Lithology is a strong control on sediment
502 composition and the underground drainage structure provides efficient pathways for
503 sediment remobilization and transport. Measures for soil erosion prevention should be
504 focused on areas with deforestation and ensuing cultivation, as well as outcropping
505 areas of intercalated clastic rock. Nevertheless, further work is required to apply source
506 fingerprinting at larger catchment scales in the karst to assess scale dependency in

507 sediment dynamics resulting from the interactions between lithology, land use and best
508 management programmes.

509

510 **Acknowledgements**

511 The work was supported by the National Key Research and Development Program
512 of China [2016YFC0502602]; the National Natural Science Foundation of China
513 [41571130074, U1612441, 41403112]; the International Partnership Project
514 [132852KYSB20170029]; and Guizhou Provincial Science and Technology
515 Department Project [(2018)5405]. [Huai Su \(Yunnan Normal University\)](#) and [Runchuan
516 Zhang \(Institute of Mountain Hazards and Environment\)](#) offered help with the
517 laboratory analyses for ^{137}Cs and magnetic susceptibility. The contribution of YZ and
518 ALC to this paper was supported by funding from UK Research and Innovation (UKRI)
519 via the Soil to Nutrition institute strategic programme grant (BBS/E/C/000I0330) from
520 the UKRI-Biotechnology and Biological Sciences Research Council (UKRI-BBSRC).

521

522 **References**

523 Ayoubi, S., Ahmadi, M., Abdi, M.R., Afshar, F.A., 2012. Relationships of Cs-137
524 inventory with magnetic measures of calcareous soils of hilly region in Iran. *Journal of
525 Environmental Radioactivity* 112, 45-51.

526 Bai, X., Zhang, X., Wang, S., Yan, D., Lihao, 2009. Estimating Sediment Deposition
527 Rates by the Cs-137 Technique in Karst Depression of Chongtou, Puding
528 County, Guizhou Province. *Earth and Environment* 37, 142-146.

529 Bonacci, O., 1987. Karst Springs. In: Bonacci, O. (Ed.), Karst Hydrology: With Special
530 Reference to the Dinaric Karst. Springer Berlin Heidelberg, Berlin, Heidelberg, pp. 49-
531 102.

532 Cao, J., Yuan, D., Tong, L., Mallik, A., Yang, H., Huang, F., 2015. An Overview of
533 Karst Ecosystem in Southwest China: Current State and Future Management. Journal
534 of Resources and Ecology 6, 247-256.

535 Chen, H., Liu, J., Zhang, W., Wang, K., 2012. Soil hydraulic properties on the steep
536 karst hillslopes in northwest Guangxi, China. Environmental Earth Sciences 66, 371-
537 379.

538 Chen, X., Chen, C., Hao, Q., Zhang, Z., Shi, P., 2008. Simulation of rainfall-
539 underground outflow responses of a karstic watershed in Southwest China with an
540 artificial neural network. Water Science and Engineering 1, 1-9.

541 Collins, A.L., Pulley, S., Foster, I.D., Gellis, A., Porto, P., Horowitz, A.J., 2017.
542 Sediment source fingerprinting as an aid to catchment management: A review of the
543 current state of knowledge and a methodological decision-tree for end-users. J Environ
544 Manage 194, 86-108.

545 Collins, A.L., Walling, D.E., 2002. Selecting fingerprint properties for discriminating
546 potential suspended sediment sources in river basins. Journal of Hydrology 261, 218-
547 244.

548 Collins, A.L., Walling, D.E., Webb, L., King, P., 2010. Apportioning catchment scale
549 sediment sources using a modified composite fingerprinting technique incorporating
550 property weightings and prior information. Geoderma 155, 249-261.

551 Collins, A.L., Zhang, Y., McChesney, D., Walling, D.E., Haley, S.M., Smith, P., 2012.
552 Sediment source tracing in a lowland agricultural catchment in southern England using
553 a modified procedure combining statistical analysis and numerical modelling. *Science*
554 *of The Total Environment* 414, 301-317.

555 Dai, Q., Liu, Z., Shao, H., Yang, Z., 2015. Karst bare slope soil erosion and soil quality:
556 a simulation case study. *Solid Earth* 6, 985-995.

557 Dai, Q., Peng, X., Yang, Z., Zhao, L., 2017. Runoff and erosion processes on bare
558 slopes in the Karst Rocky Desertification Area. *Catena* 152, 218-226.

559 Feng, T., Chen, H., Wang, K., Zhang, W., Qi, X., 2014. Modeling soil erosion using a
560 spatially distributed model in a karst catchment of northwest Guangxi, China. *Earth*
561 *Surface Processes and Landforms* 39, 2121-2130.

562 Foster, I.D.L., Lees, J.A., 1999. Changes in the physical and geochemical properties of
563 suspended sediment delivered to the headwaters of LOIS river basins over the last 100
564 years: a preliminary analysis of lake and reservoir bottom sediments. *Hydrol. Process.*
565 13, 1067-1086.

566 Fu, Z.Y., Chen, H.S., Zhang, W., Xu, Q.X., Wang, S., Wang, K.L., 2015. Subsurface
567 flow in a soil-mantled subtropical dolomite karst slope: A field rainfall simulation study.
568 *Geomorphology* 250, 1-14.

569 Gellis, A.C., Walling, D.E., 2011. Sediment Source Fingerprinting (Tracing) and
570 Sediment Budgets as Tools in Targeting River and Watershed Restoration Programs.
571 *Journal of Endovascular Therapy An Official Journal of the International Society of*
572 *Endovascular Specialists* 194, 263-291.

573 Gennadiev, A.N., Olson, K.R., Chernyanskii, S.S., Jones, R.L., 2002. Quantitative
574 assessment of soil erosion and accumulation processes with the help of a technogenic
575 magnetic tracer. *Eurasian Soil Science* 35, 17-29.

576 Hartmann, A., Goldscheider, N., Wagener, T., Lange, J., Weiler, M., 2014. Karst water
577 resources in a changing world: Review of hydrological modeling approaches. *Reviews*
578 *of Geophysics* 52, 218-242.

579 He, Q., Walling, D.E., 1996. Interpreting particle size effects in the adsorption of Cs-
580 137 and unsupported Pb-210 by mineral soils and sediments. *Journal of Environmental*
581 *Radioactivity* 30, 117-137.

582 He, Y., LI, H., Zhang, X., Yan, D., Wen, A., 2009. ¹³⁷Cs method study on soil erosion
583 and sediment yield in grass-covered peak cluster depression in Maolan, Guizhou.
584 *Carsologica Sinica* 28, 181-188.

585 Herman, E.K., Toran, L., White, W.B., 2012. Clastic sediment transport and storage in
586 fluviokarst aquifers: an essential component of karst hydrogeology. *Carbonates and*
587 *Evaporites* 27, 211-241.

588 Herman, J.S., 2012. Water Chemistry in Caves. In: White, W.B., Culver, D.C. (Eds.),
589 *Encyclopedia of Caves (Second Edition)*. Academic Press, Amsterdam, pp. 881-887.

590 Jiang, Z., Lian, Y., Qin, X., 2014a. Rocky desertification in Southwest China: Impacts,
591 causes, and restoration. *Earth-Science Reviews* 132, 1-12.

592 Jiang, Z., Luo, W., Deng, Y., Cao, J., Qin, X., Li, Y., Yang, Q., 2014b. The Leakage of
593 Water and Soil in the Karst Peak Cluster Depression and Its Prevention and Treatment.
594 *Acta Geoscientia Sinica* 35, 535-542.

595 Jintao, T.R.X.Z.X., 2004. Grain for Green Project, Grain Policy and Sustainable
596 Development [J]. *Social Sciences In China* 6.

597 Jordanova, D., Jordanova, N., Petrov, P., 2014. Pattern of cumulative soil erosion and
598 redistribution pinpointed through magnetic signature of Chernozem soils. *CATENA*
599 120, 46-56.

600 Li, S., Wu, H., 2015. Mapping karst rocky desertification using Landsat 8 images.
601 *Remote Sensing Letters* 6, 657-666.

602 Li, Y., Hou, J., Xie, D., 2002. The Recent Development of Research on Karst Ecology
603 in Southwest China. *Scientia Geographica Sinica* 22, 363-370.

604 Li, Z., Xu, X., Liu, M., Li, X., Zhang, R., Wang, K., Xu, C., 2017. State-space
605 prediction of spring discharge in a karst catchment in southwest China. *Journal of*
606 *Hydrology* 549, 264-276.

607 Li, Z., Xu, X., Zhu, J., Xu, C., Wang, K., 2019. Sediment yield is closely related to
608 lithology and landscape properties in heterogeneous karst watersheds. *Journal of*
609 *Hydrology* 568, 437-446.

610 Lin, C., Zhu, A., 1999. A Study on Soil Erosion and Prevention in Karst Mountainous
611 Region of Guizhou. *Research of Soil and Water Conservation* 6, 109-113.

612 Lu, S., 2003. *Chinese Soil Magnetism and Environment*. Higher education press.

613 Mararakanye, N., Sumner, P.D., 2017. Gully erosion: A comparison of contributing
614 factors in two catchments in South Africa. *Geomorphology* 288, 99-110.

615 Martin, J.B., Kurz, M.J., Khadka, M.B., 2016. Climate control of decadal-scale
616 increases in apparent ages of eogenetic karst spring water. *Journal of Hydrology* 540,

617 988-1001.

618 Matisoff, G., Bonniwell, E.C., Whiting, P.J., 2002. Soil erosion and sediment sources
619 in an Ohio watershed using beryllium-7, cesium-137, and lead-210. *Journal of*
620 *Environmental Quality* 31, 54-61.

621 Miller, J.R., Mackin, G., Miller, S.M.O., 2015. Application of Geochemical Tracers to
622 Fluvial Sediment.

623 Ministry of water resources, C.a.o.s., Chinese academy of engineering, 2010. Soil
624 erosion control and ecological safety in China. Science Press, Beijing.

625 Nagle, G.N., Ritchie, J.C., 2004. Wheat field erosion rates and channel bottom sediment
626 sources in an intensively cropped northeastern oregon drainage basin. *Land*
627 *Degradation & Development* 15, 15-26.

628 Ni, L.S., Fang, N.F., Shi, Z.H., Chen, F.X., Wang, L., 2017. VALIDATING A BASIC
629 ASSUMPTION OF USING CESIUM-137 METHOD TO ASSESS SOIL LOSS IN A
630 SMALL AGRICULTURAL CATCHMENT. *Land Degradation & Development* 28,
631 1772-1778.

632 Nosrati, K., Collins, A.L., 2019. Investigating the importance of recreational roads as a
633 sediment source in a mountainous catchment using a fingerprinting procedure with
634 different multivariate statistical techniques and a Bayesian un-mixing model. *Journal*
635 *of Hydrology* 569, 506-518.

636 Olson, K.R., Gennadiyev, A.N., Jones, R.L., Chernyanskii, S., 2002. Erosion patterns
637 on cultivated and reforested hillslopes in Moscow region, Russia. *Soil Sci. Soc. Am. J.*
638 66, 193-201.

639 Owens, P.N., Blake, W.H., Gaspar, L., Gateuille, D., Koiter, A.J., Lobb, D.A.,
640 Peticrew, E.L., Reiffarth, D.G., Smith, H.G., Woodward, J.C., 2016. Fingerprinting
641 and tracing the sources of soils and sediments: Earth and ocean science,
642 geoarchaeological, forensic, and human health applications. *Earth-Science Reviews*
643 162, 1-23.

644 Palazón, L., Latorre, B., Gaspar, L., Blake, W.H., Smith, H.G., Navas, A., 2015.
645 Comparing catchment sediment fingerprinting procedures using an auto-evaluation
646 approach with virtual sample mixtures. *Science of The Total Environment* 532, 456-
647 466.

648 Peng, J., Xu, Y.Q., Cai, Y.L., Xiao, H.L., 2011. The role of policies in land use/cover
649 change since the 1970s in ecologically fragile karst areas of Southwest China: A case
650 study on the Maotiaohe watershed. *Environmental Science & Policy* 14, 408-418.

651 Peng, J., Xu, Y.Q., Zhang, R., Xiong, K.N., Lan, A.J., 2013. Soil erosion monitoring
652 and its implication in a limestone land suffering from rocky desertification in the
653 Huajiang Canyon, Guizhou, Southwest China. *Environmental Earth Sciences* 69, 831-
654 841.

655 Peng, T., Wang, S., Zhang, X., Rong, L., Yang, T., Chen, B., Wang, J., 2008. RESULTS
656 OF PRELIMINARY MONITORING OF SURFACE RUNOFF COEFFICIENTS FOR
657 KARST SLOPES. *Earth and Environment* 36, 125-129.

658 Peng, T., Wang, S.J., 2012. Effects of land use, land cover and rainfall regimes on the
659 surface runoff and soil loss on karst slopes in southwest China. *Catena* 90, 53-62.

660 Poesen, J., Nachtergaele, J., Verstraeten, G., Valentin, C., 2003. Gully erosion and

661 environmental change: importance and research needs. *Catena* 50, 91-133.

662 Pulley, S., Collins, A.L., 2018. Tracing catchment fine sediment sources using the new
663 SIFT (Sediment Fingerprinting Tool) open source software. *Science of The Total*
664 *Environment* 635, 838-858.

665 Rahimi, M.R., Ayoubi, S., Abdi, M.R., 2013. Magnetic susceptibility and Cs-137
666 inventory variability as influenced by land use change and slope positions in a hilly,
667 semiarid region of west-central Iran. *Journal of Applied Geophysics* 89, 68-75.

668 Rousseeuw, P.J., Croux, C., 1993. ALTERNATIVES TO THE MEDIAN ABSOLUTE
669 DEVIATION. *J. Am. Stat. Assoc.* 88, 1273-1283.

670 Russell, M.A., Walling, D.E., Hodgkinson, R.A., 2001. Suspended sediment sources in
671 two small lowland agricultural catchments in the UK. *Journal of Hydrology* 252, 1-24.

672 Sadiki, A., Faleh, A., Navas, A., Bouhlassa, S., 2009. Using magnetic susceptibility to
673 assess soil degradation in the Eastern Rif, Morocco. *Earth Surface Processes and*
674 *Landforms* 34, 2057-2069.

675 Theuring, P., Collins, A.L., Rode, M., 2015. Source identification of fine-grained
676 suspended sediment in the Kharaa River basin, northern Mongolia. *Science of the Total*
677 *Environment* 526, 77-87.

678 Wan, G., Lin, W., Huang, R., Chen, Z., 1991. Dating characteristics and erosion traces
679 of ¹³⁷Cs vertical profiles in Hongfeng Lake sediments. *Chinese Science Bulletin* 36,
680 674-674.

681 Wang, F., Li, R., Yang, Q., 2003. Review on Effects of Human Activities on the Soil
682 Erosion in the Loess Plateau. *Journal of Sediment Research* 0, 74-80.

683 Wang, J., Zou, B., Liu, Y., Tang, Y., Zhang, X., Yang, P., 2014. Erosion-creep-collapse
684 mechanism of underground soil loss for the karst rocky desertification in Chenqi village,
685 Puding county, Guizhou, China. *Environmental Earth Sciences* 72, 2751-2764.

686 Wei, X., 2013. Monitoring of soil erosion and nutrient loss on the mountain slope in
687 karst valley region based on isotope. *Transactions of the Chinese Society of*
688 *Agricultural Engineering* 29, 128-136.

689 Wei, X., Yan, Y., Xie, D., Ni, J., Loaiciga, H.A., 2016. The soil leakage ratio in the
690 Mudu watershed, China. *Environmental Earth Sciences* 75.

691 Wenbo, W., Yunlong, C.A.I., Hongya, W., 2008. Dating by sediment grain size and
692 ^{137}Cs in small reservoir: a case study of Kechou reservoir, in Karst area of central
693 Guizhou Province. *Scientia Limnologica Sinica* 20, 306-314.

694 White, W.B., 2007. Brief history of karst hydrogeology: Contributions of the NSS. *J.*
695 *Cave Karst Stud.* 69, 13-26.

696 Wilcox, B.P., Wilding, L.P., Woodruff, C.M., 2007. Soil and topographic controls on
697 runoff generation from stepped landforms in the Edwards Plateau of Central Texas.
698 *Geophys. Res. Lett.* 34, 6.

699 Williams, P.W., 1983. The role of the subcutaneous zone in karst hydrology. *Journal of*
700 *Hydrology* 61, 45-67.

701 Yuan, D., 1997. Rock desertification in the subtropical karst of south China. *Zeitschrift*
702 *fur Geomorphologie* 108.

703 Zhang, X.-N., Wang, K.-L., Zhang, W., Chen, H.-S., He, X.-Y., Zhang, X.-B., 2009.
704 Distribution of ^{137}Cs and relative influencing factors on typical karst sloping land.

705 Huan jing ke xue= Huanjing kexue 30, 3152-3158.

706 Zhang, X., Bai, X., Liu, X., 2011. Application of a Cs-137 fingerprinting technique for
707 interpreting responses of sediment deposition of a karst depression to deforestation in
708 the Guizhou Plateau, China. Science China-Earth Sciences 54, 431-437.

709 Zhang, X., Wang, S., Cao, J., Wang, K., Meng, T., Bai, X., 2010. Characteristics of
710 water loss and soil erosion and some scientific problems on karst rocky desertification
711 in Southwest China karst area. Carsologica Sinica 29, 274-279.

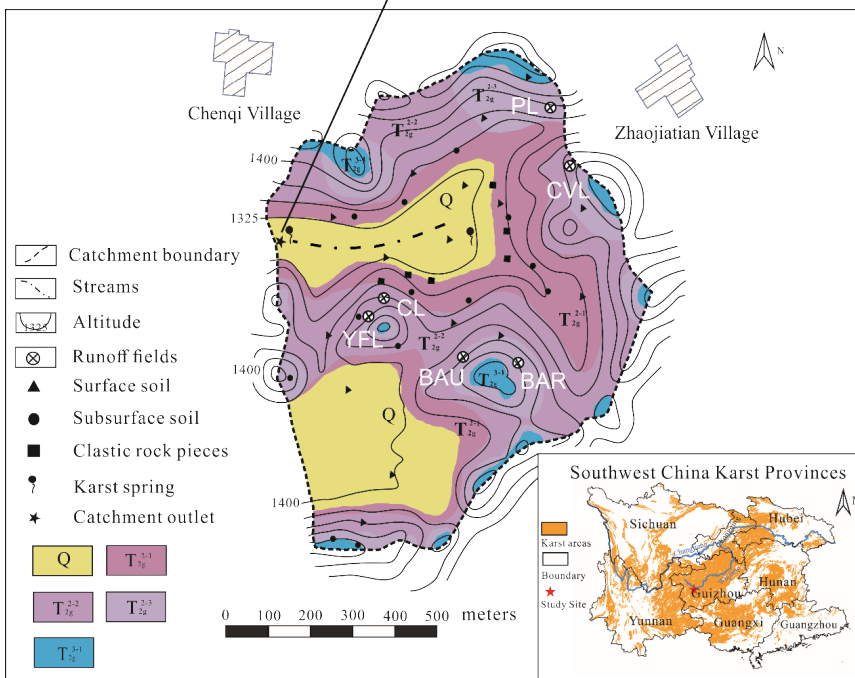
712 Zhang, X., Wang, S., He, X., Wang, Y., He, Y., 2007. SOIL CREEPING IN
713 WEATHERING CRUSTS OF CARBONATE ROCKS AND UNDERGROUND SOIL
714 LOSSES ON KARST SLOPES. Earth and Environment 35, 202-206.

715 Zhang, Z.C., Chen, X., Huang, Y.Y., Zhang, Y.F., 2014. Effect of catchment properties
716 on runoff coefficient in a karst area of southwest China. Hydrol. Process. 28, 3691-
717 3702.

718 Zhao, G., Klik, A., Mu, X., Wang, F., Gao, P., Sun, W., 2015. Sediment yield estimation
719 in a small watershed on the northern Loess Plateau, China. Geomorphology 241, 343-
720 352.

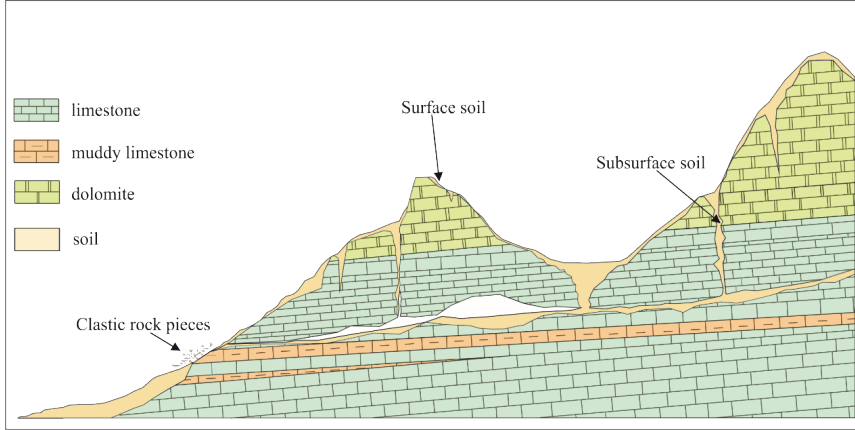
721 Zhao, G., Mu, X., Han, M., An, Z., Gao, P., Sun, W., Xu, W., 2017. Sediment yield and
722 sources in dam-controlled watersheds on the northern Loess Plateau. CATENA 149,
723 110-119.

724 Zhou, J., Tang, Y., Yang, P., Zhang, X., Zhou, N., Wang, J., 2012. Inference of creep
725 mechanism in underground soil loss of karst conduits I. Conceptual model. Natural
726 Hazards 62, 1191-1215.

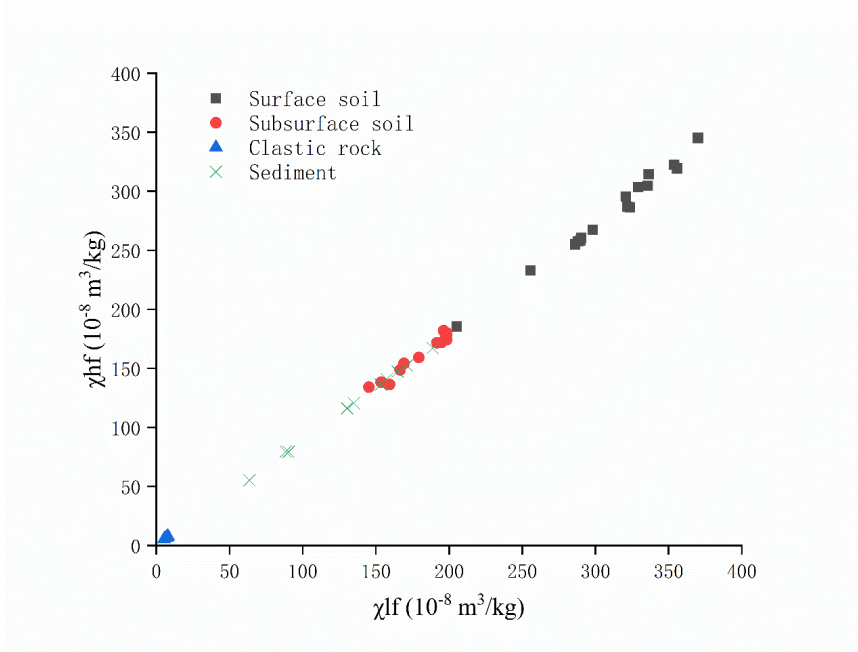


727

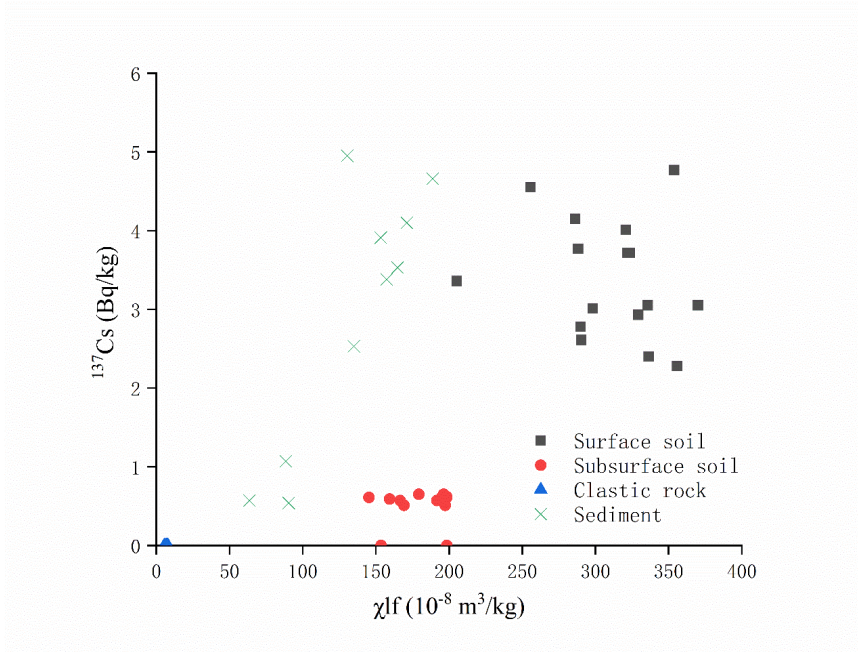
728 Figure 1



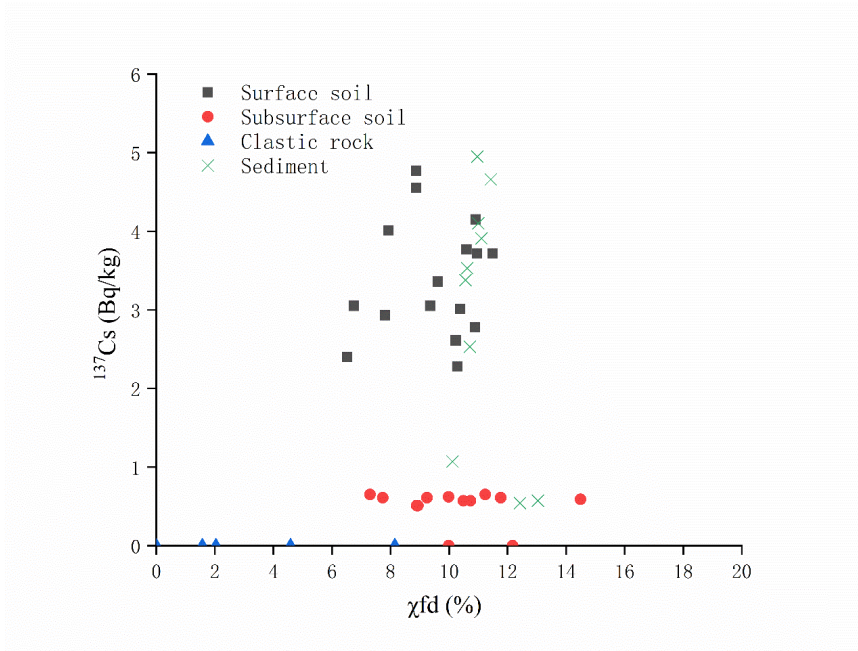
729
 730 Figure 2
 731
 732
 733
 734
 735
 736
 737
 738
 739
 740
 741
 742
 743
 744
 745



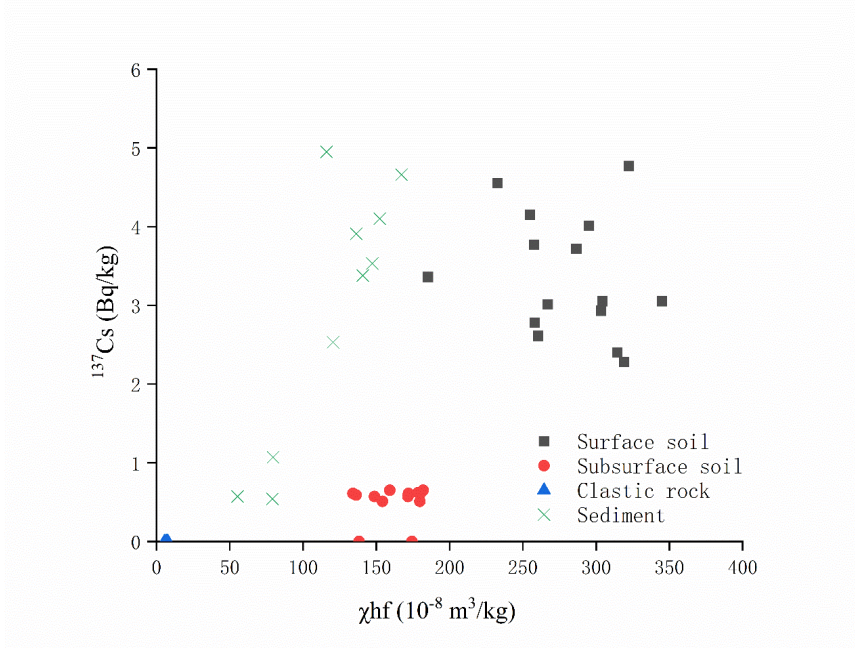
746
 747 Figure 3
 748
 749
 750



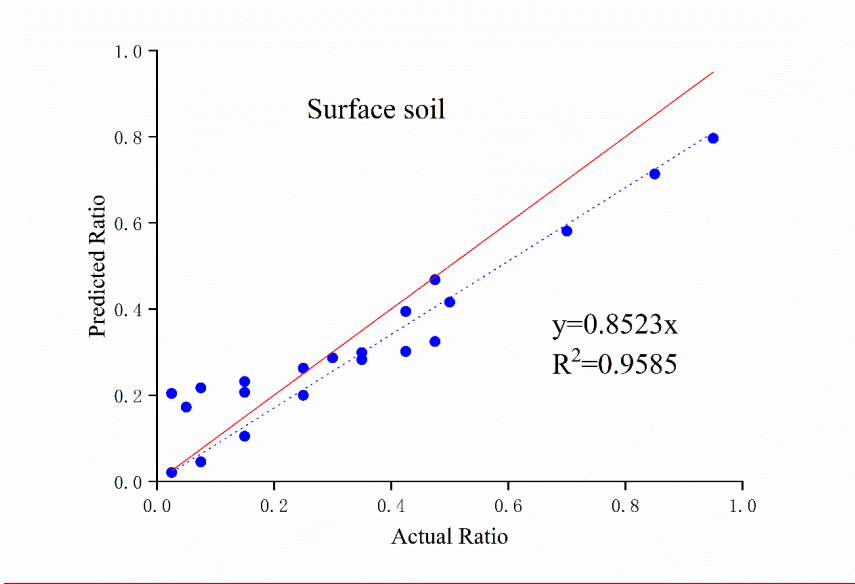
751
752 Figure 4a



753
754 Figure 4b

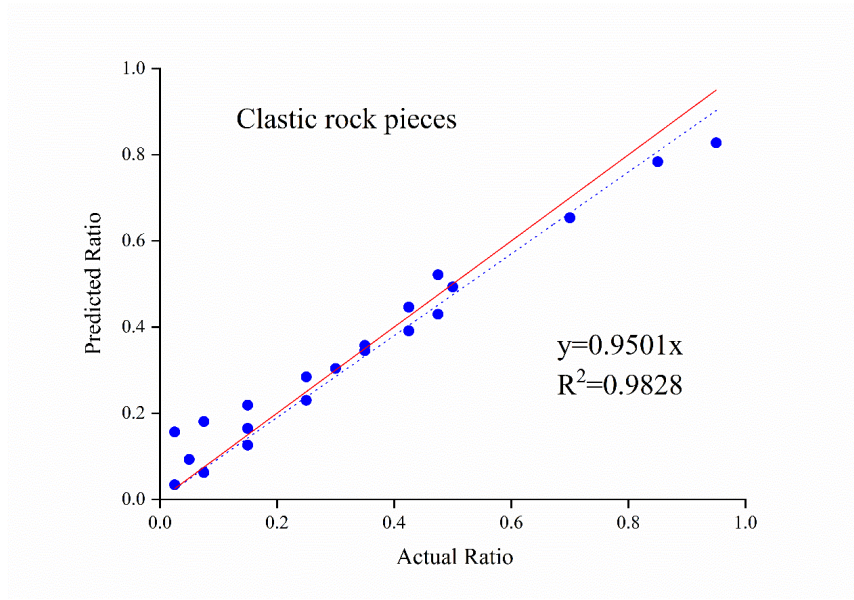


755
 756 Figure 4c
 757
 758 a)

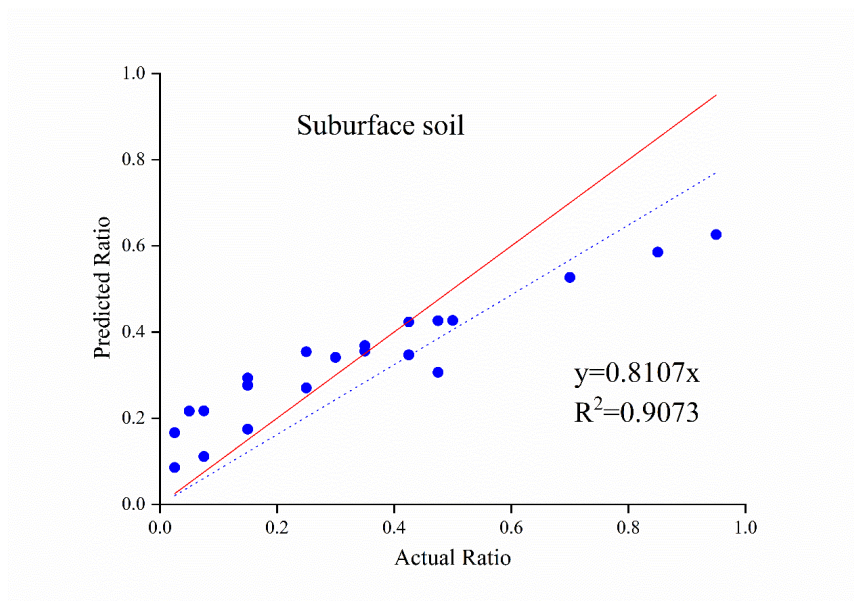


759
 760

761 b)

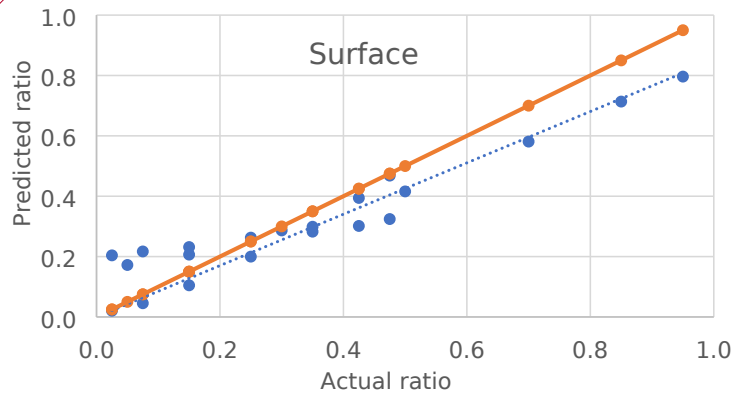


762
763
764 c)



765
766 Figure 5

767
768 a)



Commented [CQ2R2]:

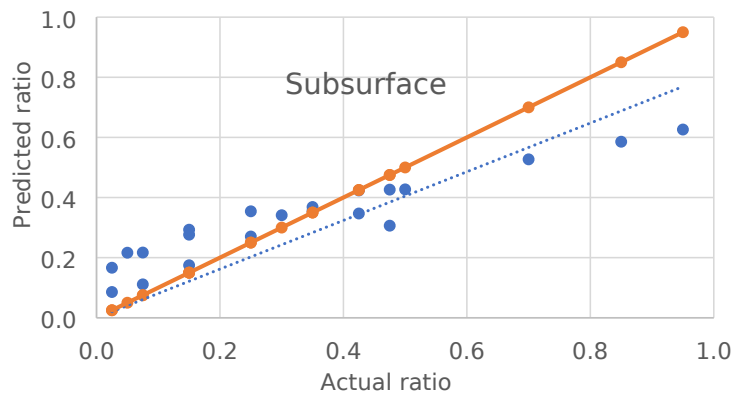
Commented [CQ1]: I want to redraw Figure 5, but I don't have the access to see the original data for the figures.

769

770

771

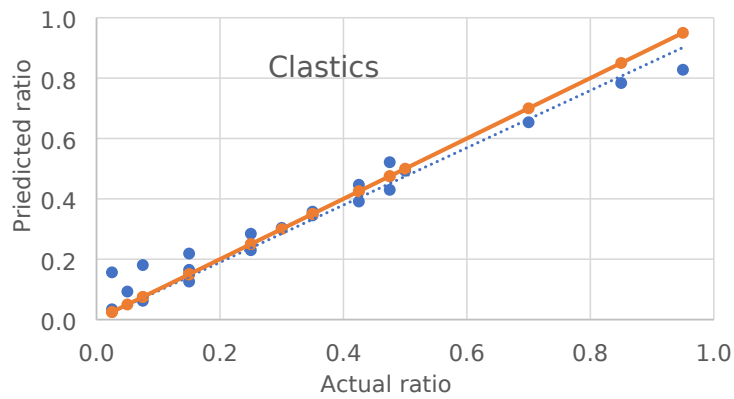
b)



772

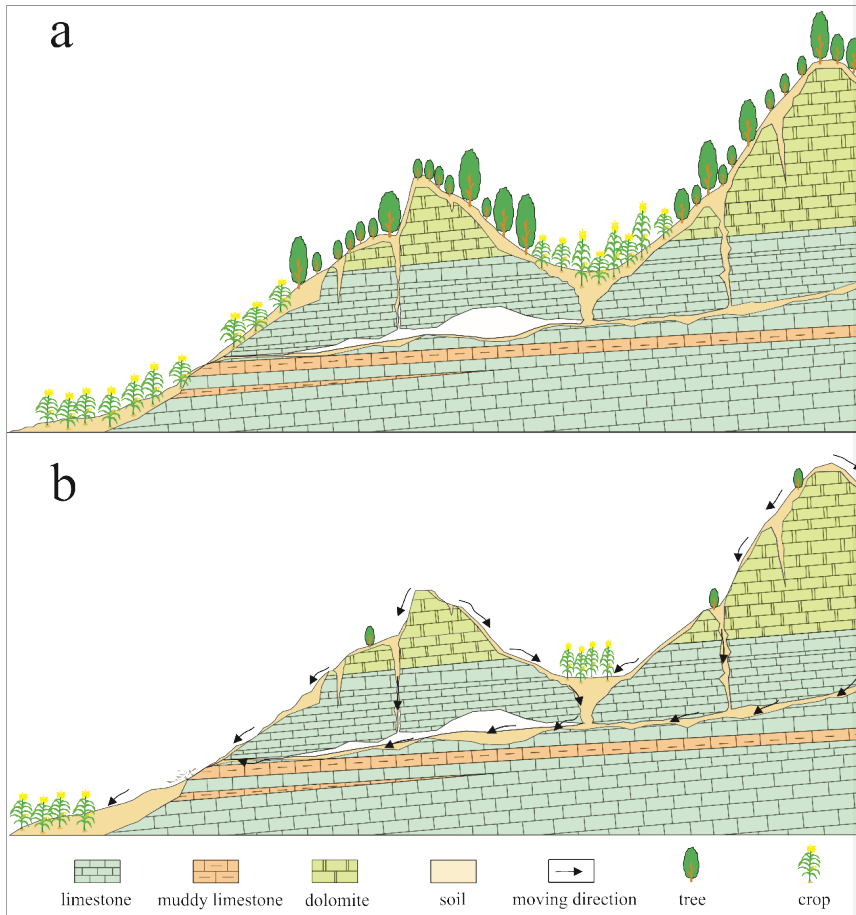
773

c)



774

775 Figure 5
776
777
778



779
780 Figure 6